Applied Physics Letters

RESEARCH ARTICLE | MARCH 17 2026

Electric field-tunable Luttinger compensated antiferromagnetism in $CrCl_2$ double chains

Deping Guo ; Weihan Zhang; Canbo Zong; Cong Wang ; Wei Ji

Appl. Phys. Lett. 128, 111602 (2026)
https://doi.org/10.1063/5.0305548

AIP Publishing

Applied Physics Letters ARTICLE pubs.aip.org/aip/apl

Electric field-tunable Luttinger compensated antiferromagnetism in $CrCl_2$ double chains

Cite as: Appl. Phys. Lett. **128**, 111602 (2026); doi: 10.1063/5.0305548
Submitted: 7 October 2025 · Accepted: 24 February 2026 ·
Published Online: 17 March 2026

Deping Guo,[1,a)] Weihan Zhang,[2,3] Canbo Zong,[2,3] Cong Wang,[2,3] and Wei Ji[2,3]

AFFILIATIONS

[1]College of Physics and Electronic Engineering, Center for Computational Sciences, Sichuan Normal University, Chengdu 610101, China
[2]Beijing Key Laboratory of Optoelectronic Functional Materials & Micro-Nano Devices, School of Physics, Renmin University of China, Beijing 100872, China
[3]Key Laboratory of Quantum State Construction and Manipulation (Ministry of Education), Renmin University of China, Beijing 100872, China

[a)]Author to whom correspondence should be addressed: dpguo@sicnu.edu.cn

ABSTRACT

Luttinger compensated antiferromagnets (LcAFMs), combining spin polarization with vanishing net magnetization, offer distinct advantages for next-generation spintronic applications. Using first-principles calculations, we demonstrate that conventional antiferromagnetic $CrCl_2$ double chains can be transformed into one-dimensional LcAFMs under an external electric field, exhibiting pronounced isotropic spin splitting. The magnitude of the splitting, as well as the bandgap, can be effectively tuned by both in-plane and out-of-plane fields, thereby providing greater controllability than in two-dimensional counterparts. To further enhance the tunability, we design a nearly lattice-matched $CrCl_2$/$MoTe_2$ heterostructure and uncover that interfacial charge transfer generates a built-in electric field, inducing spin splitting comparable to that driven by external fields. These results establish interfacial engineering as a highly efficient route to realize and manipulate LcAFM states in low-dimensional magnets, expanding the design principles for spintronic functionalities at the nanoscale.

Conventional antiferromagnets (AFM) are appealing platforms for ultrahigh-density spintronic integration because their negligible stray fields suppress magnetic crosstalk.[1] However, the absence of net magnetization hinders conventional routes to spin-polarized charge currents and complicates electrical readout, although spin–orbit and interfacial effects can partially alleviate these limitations. Recently, altermagnets have been identified as collinear magnets that retain zero net magnetization yet host momentum-dependent spin polarization without requiring relativistic spin–orbit coupling.[2,3] The spin polarization arises from spin group symmetries that break the joint parity-time (P-T) or time-reversal-fraction-translation (Tτ) symmetry. When these symmetries are further lifted, the altermagnetic state evolves into a Luttinger-compensated antiferromagnet (LcAFM), which exhibits isotropic spin splitting[4–6] across the entire Brillouin zone (BZ). LcAFMs remain collinear and magnetically compensated but exhibit spin polarization[5–8] that displays anomalous Hall and magneto-optical responses even in the absence of spin–orbit coupling.[5] The exact magnetic compensation in LcAFMs is not protected by symmetry but arises from electron filling, which ensures an exact balance between spin-up and spin-down occupations despite the presence of localized magnetic moments.[9–20] Because the opposite-spin sublattices are not symmetry-related, LcAFMs can be robust against external perturbations.

Extending the family of LcAFMs from three dimensions into low-dimensional materials opens promising avenues for tunable quantum functionalities and integration into nanoscale spintronic devices. Numerous altermagnets have been theoretically proposed and some experimentally verified,[21,22] the number of predicted LcAFMs in bulk materials remains limited,[4,7,8,15,20,23] and even fewer candidates have been predicted in two dimensions.[5,24,25] A recent theoretical study suggests that 2D LcAFMs could be realized by lifting the symmetries that relate the two spin sublattices through Janus structures, electric field- or substrate-induced staggered potentials, or elemental substitution.[5] These strategies render the two spin sublattices symmetry-unrelated, thereby exhibiting spin splitting across entire BZ. One-dimensional (1D) single-atomic magnetic chains were recently synthesized in experiments,[26–30] establishing them as an emerging member of the low-dimensional magnet family. Their interchain interactions are

governed by similar mechanisms to interlayer couplings in 2D magnets, sharing the same features of highly tunable and strongly influential on the overall magnetism. In our previous work, we theoretically demonstrated the emergence of altermagnetic states in quasi-one-dimensional layered structures self-assembled from 1D magnetic atomic chains.[31] This naturally raises a question: can assembled 1D magnetic chain structures host LcAFMs?

In this work, we theoretically explore the magnetic properties of experimentally synthesized AFM $CrCl_2$ double chains[27] under external electric fields. Using density functional theory (DFT) calculations, we reveal that the application of an electric field breaks both the inversion symmetry and $\{C_{2x}|(1/2,0,0)\}$ symmetry operation connecting opposite sublattices, thereby driving a phase transition into an LcAFM state characterized by pronounced isotropic spin splitting. The spin splitting magnitude and the bandgap can be effectively tuned by the electric field strength. To realize a permanent electric field, we further construct a heterostructure of $CrCl_2$ double chains on a nearly lattice-matched $MoTe_2$ substrate, where the substrate-induced built-in field stabilizes the LcAFM states.

Our DFT calculations were carried out using the generalized gradient approximation for the exchange–correlation potential,[32] the projector augmented wave method[33] and a plane wave basis set as implemented in the Vienna *ab initio* simulation package (VASP).[34,35] In all calculations, the Grimme's D3 form vdW correction was applied to the Perdew–Burke–Ernzerhof (PBE) exchange functional (PBE-D3).[36] Kinetic energy cutoffs of 700 and 500 eV for the plane wave basis set were used in structural relaxations and electronic calculations, respectively. The structures were fully relaxed until the residual force per atom was less than 0.001 (0.01) eV/Å for free-standing (substrate-supported) $CrCl_2$ double chains. A $22 \times 1 \times 1$ ($14 \times 2 \times 1$) k-mesh was adopted to sample the Brillouin zone of free-standing (substrate-supported) $CrCl_2$ double chains. A vacuum layer, over 15 Å in thickness, was used to reduce interactions among image slabs. On-site Coulomb interactions on the Cr d orbitals were considered using a DFT+U method[37] with $U = 6.2$ eV and $J = 1.0$ eV, consistent with the values used in the literature.[27] Phonon spectra were calculated using the density functional perturbation theory, as implemented in the PHONOPY code.[38] In phonon spectrum calculation, the dispersion correction was made at the van der Waals density functional (vdW-DF) level[39] with the optB86b functional for the exchange potential (optB86b-vdW).[40] The external electric field was simulated by applying a linear potential within the dipole correction scheme implemented in VASP.[41] In constructing the $CrCl_2/MoTe_2$ heterostructure, a bilayer $MoTe_2$ substrate was adopted. During structural relaxation, the bottom layer of $MoTe_2$ was fixed, while the top layer and the $CrCl_2$ double chains were fully relaxed.

To realize 1D LcAFM states through the construction of double-chain structures, it is first required that the total magnetic moment of the double chain vanishes. This condition necessitates AFM ordering either within each chain or between the chains. The stable phase of 1D $CrCl_2$ is the α-phase.[42] When two $CrCl_2$ chains are combined to form a double chain, the periodic axis is oriented along the x-direction [Figs. 1(a) and 1(b)], along which the double-chain structure was constructed and fully relaxed. The two chains adopt a staggered stacking, with Cr atoms facing the Cl atoms of the adjacent chain [Figs. 1(a)–1(c)], rather than a direct AA stacking, which exhibits imaginary phonon frequencies. Considering five magnetic configurations [Figs. 1(a)–1(g)], we find that the magnetic ground state corresponds to intrachain FM and interchain AFM (AFM1) [Fig. 1(a)]. This configuration remains energetically preferred across the range of Hubbard U values considered [Fig. 1(h) and Fig. S1]. In this magnetic ground-state configuration, the intrachain lattice constant is 3.52 Å, and the interchain distance is 2.88 Å [Figs. 1(b) and 1(c)], which is larger than the Cr–Cl bond length (2.53 Å) in 2D $CrCl_2$. The easy axis of magnetization lies along the z-direction, with a magnetic anisotropy energy of 1.1 meV/Cr [Fig. 1(i)]. The phonon spectrum exhibits no significant imaginary frequencies [Fig. 1(g)], confirming the dynamical stability of the double chain.

The space group of the $CrCl_2$ double chains is $P2_1/m$ (No. 11). Sublattices with opposite spins are related through either inversion symmetry or the operation $\{C_{2x}|(1/2,0,0)\}$, thereby ensuring PT

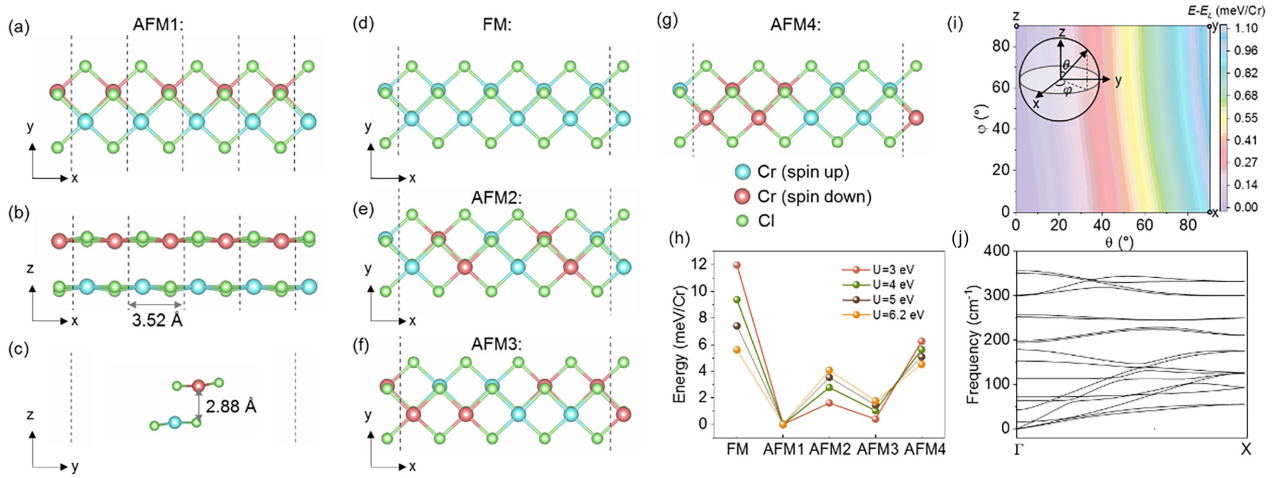

FIG. 1. (a) Top and (b) and (c) side views of $CrCl_2$ double chains under AFM1 magnetic configuration. (d)–(g) Top views of $CrCl_2$ double chains under (d) FM, (e) AFM2, (f) AFM3, and (g) AFM4 magnetic configurations. (h) Relative energies of five magnetic configurations as a function of U at $J = 1.0$ eV. (i) Magnetic anisotropy energy mapping of $CrCl_2$ double chains with the AFM1 configuration. The coordinate system was defined as shown. The zero energy is defined by the configuration in which the magnetic moments align parallel to the z-direction. (j) Phonon spectra of $CrCl_2$ double chains with the AFM1 configuration.

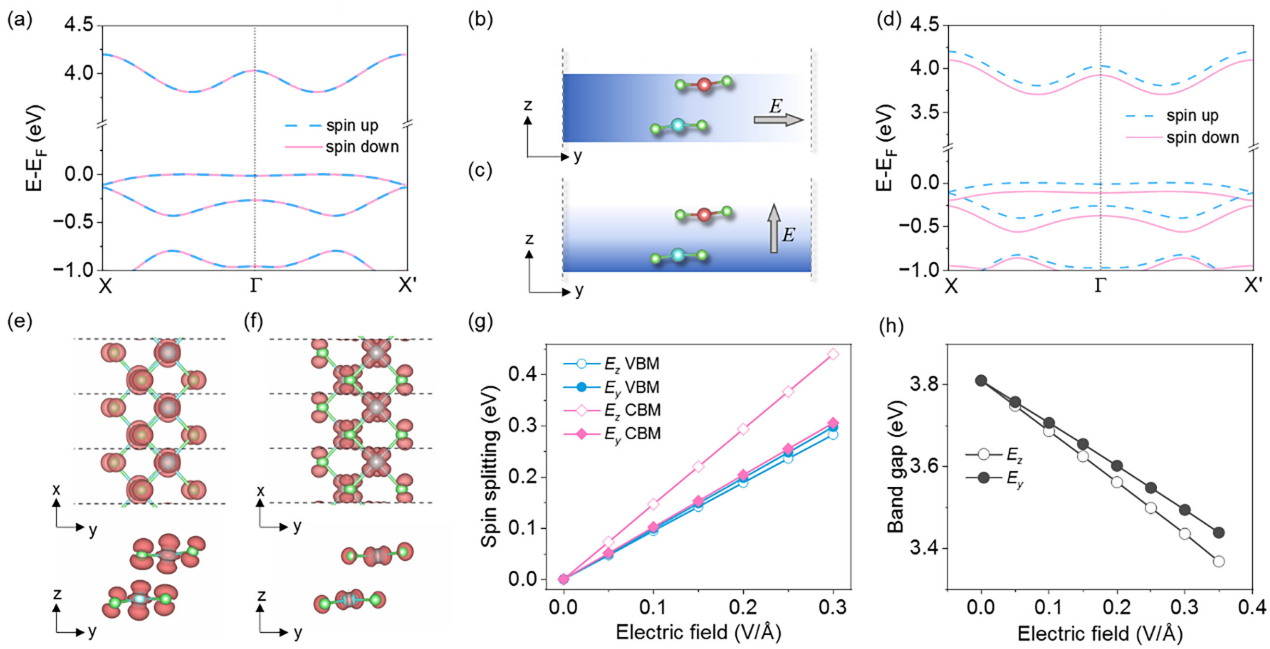

FIG. 2. (a) Band structure of the $CrCl_2$ double chains under the AFM1 configuration. (b) and (c) Schematic illustration of an external electric field applied along the (b) *y*- and (c) z-directions of the $CrCl_2$ double chains. (d) Band structure of the $CrCl_2$ double chains under an external electric field of $E_y = 0.1$ V/Å. (e) and (f) Plots of wavefunction norms for the (e) valence band maximum (VBM) and (f) conduction band minimum (CBM) at the Γ point. (g) and (h) Variation of the (g) spin splitting at the VBM and CBM, and (h) the bandgap as a function of the external electric field.

symmetry and classifying the system as a conventional AFM. From the band structure [Fig. 2(a)], it is evident that the spin-up and spin-down states remain degenerate, with a bandgap of 3.81 eV, which is in good agreement with the value of 3.87 eV calculated using the HSE06 functional (Fig. S2). Given that the influence of the external electric field on the lattice constants of the $CrCl_2$ double chains is negligible (Fig. S3), we primarily focused on its impact on the electronic states, with the lattice constants kept fixed in the subsequent calculations. Upon the application of either an in-plane or out-of-plane electric field [Figs. 2(b) and 2(c)], however, both the inversion symmetry and the $\{C_{2x}|(1/2,0,0)\}$ operation in the $CrCl_2$ double chains are broken as a result of the electrostatic potential difference. Consequently, the sublattices with opposite spins are no longer connected through any symmetry operation, leading to the emergence of LcAFM states.

In comparison with two-dimensional (2D) LcAFM systems, the 1D LcAFM not only permits the modulation of its electronic states through an out-of-plane electric field but also allows for precise control via an in-plane field, thereby providing an additional degree of tunability. When an in-plane electric field of 0.1 V/Å is applied, an isotropic spin splitting emerges, with a magnitude of approximately 100 meV at the valence band maximum [Fig. 2(d)]. Concomitantly, the bandgap is reduced to 3.71 eV from 3.81 eV.

Furthermore, the simultaneous application of a 5 T magnetic field and an electric field ($E_y = 0.1$ V/Å) confirms that the electronic structure is dominated by the electric field, with the magnetic field having no significant impact (Fig. S4).

To clarify the relationship between spin splitting and electric field orientation, we analyzed the partial charge densities (PCD) of the band edges at the Γ point [Figs. 2(e) and 2(f)]. The valence band maximum (VBM) originates mainly from out-of-plane Cr-dz^2/Cl-p_z orbitals [Fig. 2(e)], while the conduction band minimum (CBM) comprises in-plane Cr-dx^2-y^2/Cl-p_x orbitals [Fig. 2(f)]. Both in-plane and out-of-plane electric fields induce analogous trends, characterized by a progressive increase in spin splitting with field strength, while the overall dispersion relations remain largely unchanged (Fig. S5). The VBM undergoes larger spin splitting under an in-plane (*y*) field [Fig. 2(g), blue lines], whereas the CBM splits more significantly under an out-of-plane (*z*) field [Fig. 2(g), pink lines]. This indicates that the magnitude of the spin splitting is closely related to the specific orbital distribution of the bands and their response to the external electric field. Under the applied field, the conduction band minimum (spin-down, pink solid line) shifts downward, while the valence band maximum (spin-up, blue dashed line) shifts upward (Fig. S6). The reduction in the bandgap is governed by the concurrent splitting of both bands; thus, larger splitting amplitudes directly result in a greater reduction of the gap. Consequently, with increasing field strength, the bandgap of the $CrCl_2$ double chains diminishes monotonically [Fig. 2(h)].

Charge transfer from the substrate can induce an intrinsic electric field, thereby offering a direct and more energy-efficient strategy for modulating the electronic structure of $CrCl_2$ double chains than the application of an external electric field. Accordingly, we designed a heterostructure with bilayer $MoTe_2$ as the substrate, selected for its lattice constant (a = 3.52 Å) commensurate with that of $CrCl_2$ (a = 3.52 Å), which minimizes potential strain effects on the electronic properties of the chains and renders experimental fabrication more feasible. The periodic axis (*x* axis) of the $CrCl_2$ chains is oriented along the zig-zag (*x* axis) direction of $MoTe_2$ ($1 \times 1 \times 1$ $CrCl_2$ chains on $1 \times 4\sqrt{3} \times 1$ $MoTe_2$). Taking into account the structural characteristics of the $CrCl_2$

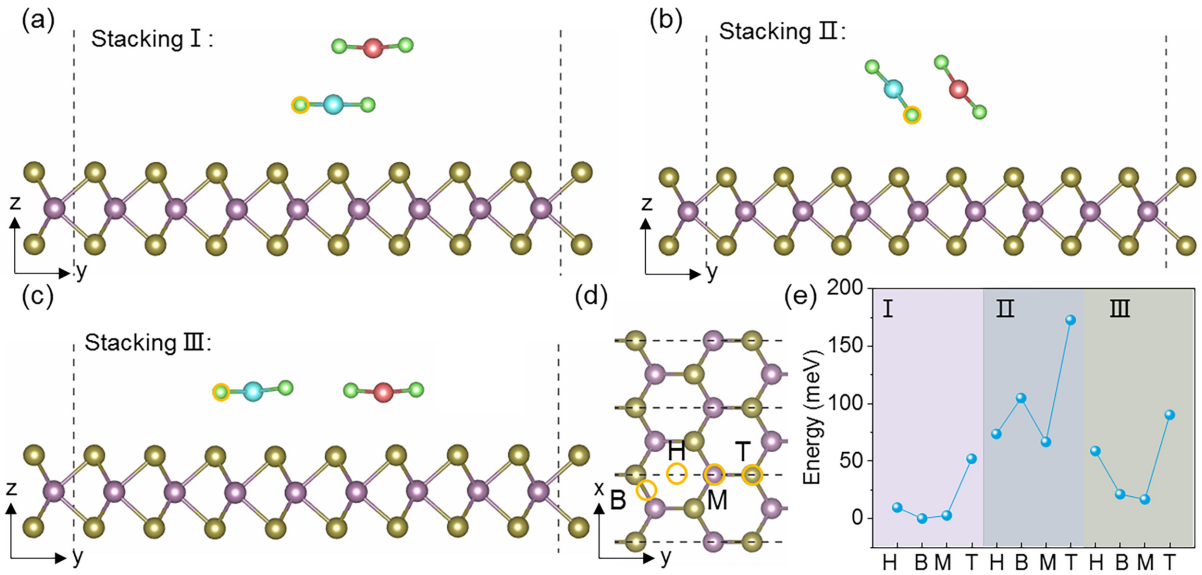

FIG. 3. (a)–(c) Side views of three stacking styles of the $CrCl_2/MoTe_2$ heterostructure: (a) vertical (I), (b) tilted-parallel (II), and (c) parallel orientations (III). A free-standing bilayer $MoTe_2$ is used in these structures with only the top layer displayed. (d) Considered four initial configurations for the Cl atom [highlighted by yellow circles in panels (a)–(c)], including bridge (B), hollow (H), Mo-top (M), and Te-top (T) sites. (e) Relative total energies of different initial configurations under different stackings.

double chains, three possible stacking styles were considered: perpendicular [stacking I, Fig. 3(a)], tilted-parallel [stacking II, Fig. 3(b)], and parallel [stacking III, Fig. 3(c)]. Each stacking style gives rise to distinct interfacial interactions between the $CrCl_2$ double chains and the $MoTe_2$ substrate. On this basis, four potential initial configurations were further evaluated for each stacking style, referenced to the position of a specific Cl atom [yellow circles in Figs. 3(a)–3(c)]: bridge, hollow, Mo-top, and Te-top sites [Fig. 3(d)]. Comparative total-energy analyses demonstrate that the most energetically favorable configuration is the fully relaxed bridge configuration in the perpendicular stacking style [Fig. 3(e) and Fig. S7]. In the most stable configuration, the strong interchain interactions within the $CrCl_2$ double chains are retained, as compared with stacking III, together with robust interfacial coupling to the substrate, in contrast to stacking II.

On the $MoTe_2$ substrate, the $CrCl_2$ double chains retain intrachain FM and interchain AFM coupling, consistent with their free-standing counterpart (Fig. S8). As shown in Fig. 4(a), the interfacial differential charge density (DCD) at the vertically stacked double-chain $CrCl_2/MoTe_2$ interface exhibits pronounced charge variation at the gap between the $MoTe_2$ substrate and the bottom $CrCl_2$ chain [Figs. 4(a) and 4(b)], exhibiting significant charge accumulation within the gap. The interfacial charge variation induces an out-of-plane polarization [Fig. 4(c)], thereby breaking the PT and rotation symmetry in a manner analogous to applied electric fields and consequently stabilizing the LcAFM state. Based on an effective area of 39.84 $Å^2$ (determined by the $MoTe_2$ zigzag and armchair lattice constants), which approximates the projected area of the $CrCl_2$ double chains, this electric polarization is calculated to be 4.30 pC/m. The projected band structure of the heterostructure further reveals a definite spin splitting of approximately 120 meV at the valence band edge spanning the whole BZ [Fig. 4(d)]. Although interfacial charge transfer leads to the formation of an interface dipole, the specific band alignment between

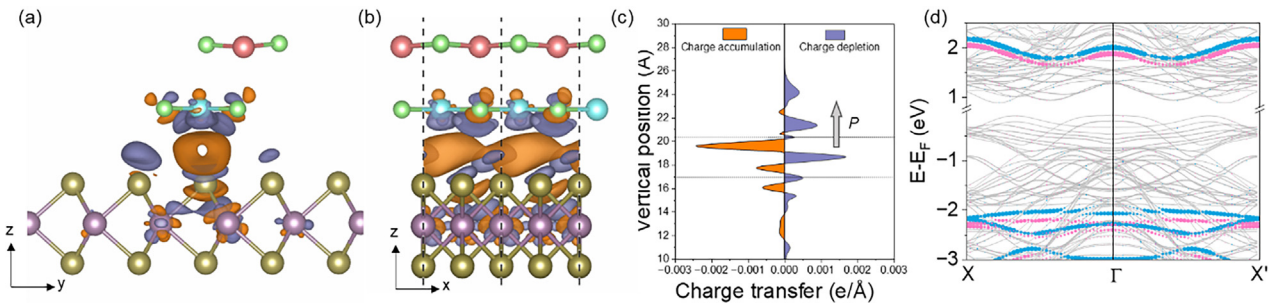

FIG. 4. (a) and (b) Side views of the differential charge density (DCD) at the $CrCl_2/MoTe_2$ interface in the most stable configuration. Orange (purple) isosurfaces represent charge accumulation (reduction). (c) The line profile of DCD along the z-direction. The gray arrow denotes the polarization induced by interfacial charge transfer. The two dashed lines indicate the highest position of Te atoms and the lowest position of Cl atoms, respectively. (d) Projected band structure of $CrCl_2/MoTe_2$ heterostructure in the most stable configuration. Blue and pink bands correspond to spin-up and spin-down states of $CrCl_2$, while gray bands mainly originate from $MoTe_2$.

the $CrCl_2$ double chains and $MoTe_2$ ensures that $CrCl_2$ retains its insulating character (Fig. S9).

Comparable isotropic spin splittings are also observed for other stacking styles (Fig. S10), although their magnitudes differ due to the stacking-dependent effective polarization induced by the varying interfacial interactions. Even with the periodic axis (x axis) of the $CrCl_2$ double chains oriented along the armchair direction of $MoTe_2$ ($7 \times 1 \times 1$ $CrCl_2$/$4 \times 7 \times 1$ $MoTe_2$), similar spin splitting arises from the built-in electric field induced by interfacial charge redistribution (Fig. S11). These results highlight the efficacy of interfacial charge transfer as a robust and versatile strategy for modulating the LcAFM state.

In summary, our study reveals that the $CrCl_2$ double chains provide a robust 1D platform for realizing field-tunable LcAFM. Unlike 2D LcAFMs, the 1D LcAFM $CrCl_2$ double chains enable the breaking of PT and $\{C_{2x}|(1/2, 0, 0)\}$ symmetries under either in-plane or out-of-plane electric fields, thereby inducing sizable isotropic spin splitting. Meanwhile, the built-in electric field induced by interfacial charge transfer in the $CrCl_2$/$MoTe_2$ heterostructure offers an alternative, energy-efficient pathway to achieve the same effect. This dual strategy, i.e., external field control and substrate-induced polarization, not only enriches the fundamental understanding of compensated magnetism in reduced dimensions but can also be extended to other thermodynamically and dynamically stable 1D antiferromagnetic nanoribbons. The demonstrated tunability and versatility highlight the potential of 1D LcAFMs as promising building blocks for future spintronic technologies.

See the supplementary material for additional details, including the energies of different magnetic configurations under varying Hubbard U values, band structures calculated using the HSE06 hybrid functional, the influence of electric and magnetic fields on lattice constants and electronic states, band structure comparisons with electric fields applied along different directions, and the structural diagrams, magnetic energies, band alignment, and electronic properties for the $CrCl_2$/$MoTe_2$ heterostructure.

We gratefully acknowledge the financial support from the National Natural Science Foundation of China (Grant Nos. 92477205 and 52461160327), the National Key R&D Program of China (Grant No. 2023YFA1406500), and the Sichuan Science and Technology Program (Grant No. 2026NSFSC0767). Calculations were performed at the Hefei Advanced Computing Center, the Physics Lab of High-Performance Computing (PLHPC), and the Public Computing Cloud (PCC) of Renmin University of China.

AUTHOR DECLARATIONS

Conflict of Interest

The authors have no conflicts to disclose.

Author Contributions

Deping Guo: Data curation (equal); Funding acquisition (equal); Investigation (equal); Supervision (equal); Writing – original draft (equal). **Weihan Zhang:** Resources (equal). **Canbo Zong:** Resources (equal). **Cong Wang:** Resources (equal). **Wei Ji:** Funding acquisition (equal); Writing – review & editing (equal).

DATA AVAILABILITY

The data that support the findings of this study are available from the corresponding author upon reasonable request.

REFERENCES

[1]V. Baltz, A. Manchon, M. Tsoi, T. Moriyama, T. Ono, and Y. Tserkovnyak, "Antiferromagnetic spintronics," Rev. Mod. Phys. **90**(1), 015005 (2018).
[2]C. Wu, K. Sun, E. Fradkin, and S.-C. Zhang, "Fermi liquid instabilities in the spin channel," Phys. Rev. B **75**(11), 115103 (2007).
[3]L. Šmejkal, J. Sinova, and T. Jungwirth, "Emerging research landscape of altermagnetism," Phys. Rev. X **12**(4), 040501 (2022).
[4]L.-D. Yuan, A. B. Georgescu, and J. M. Rondinelli, "Nonrelativistic spin splitting at the Brillouin zone center in compensated magnets," Phys. Rev. Lett. **133**(21), 216701 (2024).
[5]Y. Liu, S.-D. Guo, Y. Li, and C.-C. Liu, "Two-dimensional fully compensated ferrimagnetism," Phys. Rev. Lett. **134**(11), 116703 (2025).
[6]I. Mazin and The PRX Editors, "Editorial: Altermagnetism—A new punch line of fundamental magnetism," Phys. Rev. X **12**(4), 040002 (2022).
[7]P.-J. Guo, H.-C. Yang, X.-Y. Hou, Z.-F. Gao, W. Ji, and Z.-Y. Lu, "Luttinger-compensated bipolarized magnetic semiconductor," Phys. Rev. B **112**(18), L180405 (2025).
[8]X.-Y. Hou, Z.-F. Gao, H.-C. Yang, P.-J. Guo, and Z.-Y. Lu, "Unconventional compensated magnetic material $LaMn_2SbO_6$," Chin. Phys. Lett. **42**(7), 070712 (2025).
[9]R. A. de Groot, "Half-metallic magnetism in the 1990s," Physica B **172**(1), 45–50 (1991).
[10]S. Wurmehl, H. C. Kandpal, G. H. Fecher, and C. Felser, "Valence electron rules for prediction of half-metallic compensated-ferrimagnetic behaviour of Heusler compounds with complete spin polarization," J. Phys.: Condens. Matter **18**(27), 6171 (2006).
[11]H. Akai and M. Ogura, "Half-metallic diluted antiferromagnetic semiconductors," Phys. Rev. Lett. **97**(2), 026401 (2006).
[12]W. E. Pickett, "Spin-density-functional-based search for half-metallic antiferromagnets," Phys. Rev. B **57**(17), 10613–10619 (1998).
[13]Y. Nie and X. Hu, "Possible half metallic antiferromagnet in a hole-doped perovskite cuprate predicted by first-principles calculations," Phys. Rev. Lett. **100**(11), 117203 (2008).
[14]K. E. Siewierska, G. Atcheson, A. Jha, K. Esien, R. Smith, S. Lenne, N. Teichert, J. O'Brien, J. M. D. Coey, P. Stamenov, and K. Rode, "Magnetic order and magnetotransport in half-metallic ferrimagnetic Mn_yRu_xGa thin films," Phys. Rev. B **104**(6), 064414 (2021).
[15]R. Stinshoff, "Completely compensated ferrimagnetism and sublattice spin crossing in the half-metallic Heusler compound $Mn_{1.5}FeV_{0.5}Al$," Phys. Rev. B **95**(6), 060410 (2017).
[16]M. Žic, K. Rode, N. Thiyagarajah, Y.-C. Lau, D. Betto, J. M. D. Coey, S. Sanvito, K. J. O'Shea, C. A. Ferguson, D. A. MacLaren, and T. Archer, "Designing a fully compensated half-metallic ferrimagnet," Phys. Rev. B **93**(14), 140202 (2016).
[17]X. Hu, "Half-metallic antiferromagnet as a prospective material for spintronics," Adv. Mater. **24**(2), 294–298 (2012).
[18]K. Özdoğan, E. ß. Sasßioğlu, and I. Galanakis, "Ab-initio investigation of electronic and magnetic properties of the 18-valence-electron fully-compensated ferrimagnetic (CrV)XZ Heusler compounds: A prototype for spin-filter materials," Comput. Mater. Sci. **110**, 77–82 (2015).
[19]K. Fleischer, N. Thiyagarajah, Y.-C. Lau, D. Betto, K. Borisov, C. C. Smith, I. V. Shvets, J. M. D. Coey, and K. Rode, "Magneto-optic Kerr effect in a spin-polarized zero-moment ferrimagnet," Phys. Rev. B **98**(13), 134445 (2018).
[20]M. E. Jamer, Y. J. Wang, G. M. Stephen, I. J. McDonald, A. J. Grutter, G. E. Sterbinsky, D. A. Arena, J. A. Borchers, B. J. Kirby, L. H. Lewis, B. Barbiellini, A. Bansil, and D. Heiman, "Compensated ferrimagnetism in the zero-moment Heusler alloy Mn_3Al," Phys. Rev. Appl. **7**(6), 064036 (2017).
[21]L. Bai, W. Feng, S. Liu, L. Šmejkal, Y. Mokrousov, and Y. Yao, "Altermagnetism: Exploring new frontiers in magnetism and spintronics," Adv. Funct. Mater. **34**(49), 2409327 (2024).
[22]C. Song, H. Bai, Z. Zhou, L. Han, H. Reichlova, J. H. Dil, J. Liu, X. Chen, and F. Pan, "Altermagnets as a new class of functional materials," Nat. Rev. Mater. **10**, 473–485 (2025).

[23]T. Kawamura, K. Yoshimi, K. Hashimoto, A. Kobayashi, and T. Misawa, "Compensated ferrimagnets with colossal spin splitting in organic compounds," Phys. Rev. Lett. **132**(15), 156502 (2024).
[24]Y. Liu, Y. Liu, X. Wang, N. Xia, G. Xu, Y. Wang, H. Wang, W. Gao, and J. Zhao, "Robust altermagnetism and compensated ferrimagnetism in $MnPX_3$-based (X=S or Se) heterostructures," Phys. Rev. Mater. **9**(10), 104406 (2025).
[25]S.-D. Guo, J. He, and Y. S. Ang, "Achieving fully compensated ferrimagnetism through two-dimensional CrI_3/$CrGeTe_3$ heterojunctions," Appl. Phys. Lett. **127**(23), 232401 (2025).
[26]S. Lu, D. Guo, Z. Cheng, Y. Guo, C. Wang, J. Deng, Y. Bai, C. Tian, L. Zhou, Y. Shi, J. He, W. Ji, and C. Zhang, "Controllable dimensionality conversion between 1D and 2D $CrCl_3$ magnetic nanostructures," Nat. Commun. **14**(1), 2465 (2023).
[27]Y. Lee, L. Li, W. Zhang, U. Choi, K. Lee, Y.-M. Kim, W. Ji, W. Zhou, K. Kim, and A. Zettl, "Robust high-spin state in one-dimensional CrX_2 (X = Cl, Br, I) at the single-chain limit," J. Am. Chem. Soc. **147**(30), 26776–26785 (2025).
[28]X. Lan, L. Geng, Z. Zhang, Y. Li, J. Yuan, C.-X. Zhou, S. Huang, Z. Hu, J. Li, C. Yang, Y. Zhang, Z. Fan, D. Tian, X. Zhao, Q. Li, and L. Kang, "Tunable synthesis of atomic one-dimensional V_xTe_y magnets within single-walled carbon nanotubes," Nat. Commun. **16**(1), 6300 (2025).
[29]Y. Lee, Y. W. Choi, K. Lee, C. Song, P. Ercius, M. L. Cohen, K. Kim, and A. Zettl, "1D magnetic MX_3 single-chains (M = Cr, V and X = Cl, Br, I)," Adv. Mater. **35**, 2307942 (2023).
[30]Y. Li, A. Li, J. Li, H. Tian, Z. Zhang, S. Zhu, R. Zhang, S. Liu, K. Cao, L. Kang, and Q. Li, "Efficient synthesis of highly crystalline one-dimensional $CrCl_3$ atomic chains with a spin glass state," ACS Nano **17**(20), 20112–20119 (2023).
[31]D. Guo, C. Zong, W. Zhang, C. Wang, J. Liu, and W. Ji, "Tunable altermagnetism via interchain engineering in parallel-assembled atomic chains," Phys. Rev. B **112**(4), L041404 (2025).
[32]J. P. Perdew, K. Burke, and M. Ernzerhof, "Generalized gradient approximation made simple," Phys. Rev. Lett. **77**(18), 3865–3868 (1996).
[33]P. E. Blöchl, "Projector augmented-wave method," Phys. Rev. B **50**(24), 17953–17979 (1994).
[34]G. Kresse and J. Furthmüller, "Efficient iterative schemes for ab initio total-energy calculations using a plane-wave basis set," Phys. Rev. B **54**(16), 11169–11186 (1996).
[35]G. Kresse and J. Furthmüller, "Efficiency of ab-initio total energy calculations for metals and semiconductors using a plane-wave basis set," Comput. Mater. Sci. **6**(1), 15–50 (1996).
[36]S. Grimme, J. Antony, S. Ehrlich, and H. Krieg, "A consistent and accurate ab initio parametrization of density functional dispersion correction (DFT-D) for the 94 elements H-Pu," J. Chem. Phys. **132**(15), 154104 (2010).
[37]V. I. Anisimov, F. Aryasetiawan, and A. I. Lichtenstein, "First-principles calculations of the electronic structure and spectra of strongly correlated systems: The LDA+ U method," J. Phys.: Condens. Matter **9**(4), 767 (1997).
[38]A. Togo and I. Tanaka, "First principles phonon calculations in materials science," Scr. Mater. **108**, 1–5 (2015).
[39]M. Dion, H. Rydberg, E. Schröder, D. C. Langreth, and B. I. Lundqvist, "Van der Waals density functional for general geometries," Phys. Rev. Lett. **92**(24), 246401 (2004).
[40]J. Klimeš, D. R. Bowler, and A. Michaelides, "Van der Waals density functionals applied to solids," Phys. Rev. B **83**(19), 195131 (2011).
[41]J. Neugebauer and M. Scheffler, "Adsorbate-substrate and adsorbate-adsorbate interactions of Na and K adlayers on Al (111)," Phys. Rev. B **46**(24), 16067–16080 (1992).
[42]L. Fu, C. Shang, S. Zhou, Y. Guo, and J. Zhao, "Transition metal halide nanowires: A family of one-dimensional multifunctional building blocks," Appl. Phys. Lett. **120**(2), 023103 (2022).